

Criticality and fragility in a quantum neural memory

Inam Ullah, Subhanullah Khan, Muhammad Noman, and Minglin Lang(郎明林)
Citation: Chin. Phys. B, 2026, 35 (**5**): 050303. DOI: 10.1088/1674-1056/ae2d36
http://cpb.iphy.ac.cn; http://iopscience.iop.org/cpb

What follows is a list of articles you may be interested in

Exact quantum algorithm for unit commitment optimization based on partially connected quantum neural networks

Jian Liu(刘键), Xu Zhou(周旭), Zhuojun Zhou(周卓俊), and Le Luo(罗乐)
Chin. Phys. B, 2025, 34 (**10**): 100303. DOI: 10.1088/1674-1056/adf4aa

Dynamics of quantum discord and geometric quantum discord in multiqubit interacting system

Xiao-Di Cheng(程晓迪), Ya-Jun Zheng(郑雅君), Meng-Jie Ran(冉梦杰), and Xiao-Yun Wang(王小云)
Chin. Phys. B, 2025, 34 (**5**): 050309. DOI: 10.1088/1674-1056/adca16

Quantum discord and its dynamics for multipartite systems

Jiaxin Luo(罗嘉欣) and Qiong Guo(郭琼)
Chin. Phys. B, 2024, 33 (**6**): 060303. DOI: 10.1088/1674-1056/ad3810

Deep learning framework for time series classification based on multiple imaging and hybrid quantum neural networks

Jianshe Xie(谢建设) and Yumin Dong(董玉民)
Chin. Phys. B, 2023, 32 (**12**): 120302. DOI: 10.1088/1674-1056/accb45

A backdoor attack against quantum neural networks with limited information

Chen-Yi Huang(黄晨猗) and Shi-Bin Zhang(张仕斌)
Chin. Phys. B, 2023, 32 (**10**): 100306. DOI: 10.1088/1674-1056/acd8ab

---

Criticality and fragility in a quantum neural memory

Inam Ullah[1], Subhanullah Khan[1], Muhammad Noman[2], and Minglin Lang(郎明林)[1,†]

[1] *CAS Center for Excellence in Biotic Interactions, College of Life Science, University of Chinese Academy of Sciences, Beijing* 100049, *China*
[2] *Department of Physics, School of Physical Science and Technology, Ningbo University, Ningbo* 315211, *China*

(Received 27 October 2025; revised manuscript received 9 December 2025; accepted manuscript online 16 December 2025)

We theoretically investigate a neural transverse-field Hopfield (NTFH) model that realizes a minimal quantum neural memory by encoding patterns in the low-energy spectrum and stationary correlations of coupled qubits. At the level of a two-neuron open quantum system, we analyze how entanglement of formation, geometric quantum discord and quantum-memory-assisted entropic uncertainty evolve under the combined action of memory interactions, transverse fields, local imperfections and Markovian dephasing. This reveals a robust trade-off: transverse driving enhances coherent processing but destabilizes stored patterns, while local asymmetries and noise rapidly erase quantum correlations. Extending the model to a four-neuron network, we show that entanglement fluctuations peak at a transverse-field-driven quantum phase transition between a memory-ordered and a paramagnetic phase, thereby linking the fragility of quantum neural memory to standard notions of quantum criticality.

Keywords: quantum neural networks, hopfield model, quantum correlations, entanglement, open quantum systems, entropic uncertainty

PACS: 03.65.Yz

DOI: 10.1088/1674-1056/ae2d36 **CSTR:** 32038.14.CPB.ae2d36

1. Introduction

The brain's stunning ability to compute is like a puzzle at the core of modern science. It usually consumes only a few watts but still outsmarts big machines in the fields of pattern recognition and abstract reasoning.[1,2] In the world of computational neuroscience, the neuron model is the standard one, considering neurons as classical information processors, switches and integrators connected through large recurrent networks.[3,4] This perspective has provided a lot of significant contributions, mainly through the development of connectionist models and artificial neural networks,[5,6] but it still does not clarify some cognitive aspects which are very contextual, such as how people deal with ambiguity, why the sequence of presentation influences the evaluations and the big question of consciousness that has been around for a long time.[7,8] The scientific community sees these discrepancies as necessitating the introduction of several frameworks that can at a single abstraction level describe the behavior while still being in tune with the empirical regularities.

A possible path to follow is quantum cognition, which suggests that the mathematical interpretation of quantum theory can serve as a more natural language for modeling human judgment and decision making without having to assume a quantum substrate in the brain literally.[9–11] In the quantum cognition perspective, one aspect of quantum superposition embraces the cognitive ambiguity where several possibilities are waiting to be chosen as a response; multiple quantum states exist and then one gets to choose during the decision-making process,[12,13] and quantum interference is used to explain the non-classical probability that includes the order effects that are observed in surveys and decision-making tasks to be very robust.[14,15] The brain is perceived as a black box with incoming data and an output of responses, the formal methods are applied to behavioral data and the issue of microscopic realization is postponed.

The uncertainties that arise while trying to interpret these formal descriptions in terms of physical mechanisms are mainly due to decoherence.[16–19] The human brain is situated in a warm, moist and very noisy environment, which has the effect of eliminating very sensitive phase relations and very short-lived quantum correlations. Still, there are some quite specific hypotheses that have been put forward, among which the orchestrated objective reduction in microtubules proposed by Penrose and Hameroff[20,21] is one example and the nuclear spin qubits in Posner molecules suggested by Fisher could have a similar effect.[22] These proposals remain unverifiable; however, they create a sharper question at the core and prompt the investigation of minimal model layouts that are very well-constrained where assumptions are made clear, parameters are adjustable and the presence of quantum effects can be determined by meticulous research.

With the intention of shedding light on this matter, we consider a neuronal element as a system of two qubits. Our aim is not to replicate the brain intricately but to develop a quantum-like equivalent of a hydrogen atom in neuroscience, a manageable and simplified model wherein one could metic-

†Corresponding author. E-mail: langml@ucas.ac.cn

© 2026 Chinese Physical Society and IOP Publishing Ltd. All rights, including for text and data mining, AI training, and similar technologies, are reserved.

ulously monitor superposition, entanglement and their interplay with noise step by step.[23,24] In this model, we can pose more precise questions such as how quantum correlations are created between neurons, how they are transformed under coherent processing in contrast to noise interruption and under what conditions they may provide any functional superiority.

In this work, we use the term quantum neural memory to denote a minimal neural-like module in which information about a pattern is encoded in the low-energy structure and stationary quantum correlations of a qubit Hamiltonian, and in which computation is realized by the controlled manipulation of those correlations. Functionally, this mirrors the role of associative memory in classical Hopfield networks:[25,26] stored patterns correspond to robust attractor-like configurations, while recall corresponds to the ability of the dynamics to return the system to one of these configurations when it is perturbed or partially specified. In the quantum case considered here, the patterns are entangled states of two or more qubits, the quality of storage is captured by measures of entanglement and discord, and the trade-off between processing and robustness is governed by the competition between memory interactions, transverse fields and environmental decoherence.

In order to relate our examination to already existing concepts in memory and computation, we refer to the Hopfield network.[25] As originally proposed, the Hopfield model is an iterative associative memory that keeps patterns and retrieves them from incomplete or damaged inputs.[26] The motion follows a descending energy function in which the patterns that are imprinted correspond to the points with a local minimum in energy, a viewpoint based on the statistical mechanics of spin glasses and energy landscapes.[27] This way of thinking brings together very nicely the style of interactions of the masses with the computation emerging from them, and it also gives the quantum extensions their natural baseline for exploring.

We enhance this architecture by incorporating a transverse magnetic field, which leads us to a transverse-field Hopfield model that is within a physically accepted area of quantum condensed matter and quantum computing.[28,29] The transverse field results in a term in the Hamiltonian that is in a non-commuting relationship with the memory interactions, thus enabling tunneling between configurations and making a global state space search more efficient. This effect is very much linked to quantum annealing,[30,31] and it shows a fundamental issue, namely, one has to be always aware of the fact that the same field that allows for coherent exploration can also disrupt stored patterns. Therefore, memory and processing must be considered together, not in isolation.

An adjustable memory structure is a distinctive element of our construction. The stored pattern is encoded through an interacting Hamiltonian that varies continuously between two limits. On one side, the interaction becomes a classical Ising-like term which favors the alignment or the anti-alignment of neuronal firing states in the spirit of the original Hopfield model. On the opposite side, it is a projector onto a maximally entangled Bell state, i.e., a completely quantum pattern. A mixing parameter, α, controls the movement of the system between these two limits. This strategy allows us to investigate how the characteristics of what is stored, classical or quantum, and the resulting dynamical response, recall robustness and perturbation susceptibility, are interrelated.

Any practical neuronal system is interacting with its environment, and thus we consider the model an open quantum system.[32] Related analyses of entanglement and uncertainty dynamics in open-system settings can be found in Refs. [33,34]. The Lindblad master equation is employed to model dissipation and dephasing; this is a well-established and robust framework for Markovian dynamics that accounts for the loss of phase information and the consequent shift towards classical behavior.[35,36] By means of this methodology, we are able to introduce environmental dephasing in the simulations and, at the same time, quantify its effect on quantum resources such as entanglement and discord, which are pivotal in quantum information processing and may rapidly get lost due to local noise.

Despite these advances, there remains a clear gap between abstract quantum-cognitive frameworks and physically explicit models of neural memory. Most work on quantum cognition uses the mathematical machinery of Hilbert spaces and quantum probabilities as an effective language for behavioral data,[9,11] without specifying how genuinely quantum resources such as entanglement or discord arise, evolve and degrade in a concrete neural-like architecture subject to decoherence. Likewise, quantum extensions of Hopfield networks and transverse-field spin-glass models typically focus either on ground-state properties or on algorithmic performance in closed systems,[28,29,37,38] rather than on the dynamical competition between memory storage, coherent processing and environmental noise in a minimal neuronal unit.

In this work, we address these gaps by introducing a neural transverse-field Hopfield (NTFH) model that treats a pair of neurons as a two-qubit open quantum system with a tunable memory Hamiltonian. The memory term interpolates continuously between a classical Hopfield-type Ising interaction and a projector onto a maximally entangled Bell state, controlled by a single mixing parameter α, which allows classical and quantum memories to be compared within the same framework. We explicitly incorporate realistic control and imperfection terms, transverse fields, local biases and XY crosstalk, and embed the system in a Markovian dephasing environment described by a Lindblad master equation.[18,32] The resulting dynamics are characterized using complementary information-theoretic diagnostics, namely, entanglement offormation,[39] geomet-

ric quantum discord,[40] and quantum-memory-assisted entropic uncertainty (EUR).[41] Finally, by extending the construction to a four-qubit network, we show that entanglement fluctuations peak at a transverse-field-driven quantum phase transition separating a memory-ordered from a paramagnetic phase.[42] Together, these elements provide a minimal yet fully specified quantum neural memory model in which the tradeoff between coherent processing and robust associative storage can be analyzed quantitatively.

To enhance clarity, we summarize the main contributions of this work as follows. First, we formulate an NTFH model that realizes a quantum neural memory as a two-qubit open quantum system with a tunable memory Hamiltonian interpolating between a classical Hopfield interaction and a Bell-state projector. Second, we characterize the competition between memory interactions, transverse fields and dephasing using three complementary information-theoretic diagnostics — entanglement of formation (EOF), geometric quantum discord (GQD) and quantum-memory-assisted entropic uncertainty — and systematically study the impact of local biases, XY crosstalk and noise strength on the fragility of quantum correlations. Third, we extend the model to a four-qubit network and show that entanglement fluctuations peak at a transverse-field-driven quantum phase transition between a memory-ordered and a paramagnetic phase, thereby linking quantum neural memory to standard notions of quantum criticality.

Next, we present a comprehensive study of the two-neuron quantum Hopfield model, where the coherent tunneling due to the transverse field, the nature of the memory to be stored, local imbalances and environmental dephasing are found to be together responsible for the evolution of the quantum correlations of the system. By monitoring the evolution of entanglement, quantum discord and entropic uncertainty, we try to indicate the main principles that govern both storage and processing in a simple quantum neural circuit. The paper is structured as follows. In Section 2, the physical model and the dynamical formalism are introduced; in Section 3, the computational measures used for the quantification of correlations and uncertainty are discussed in detail; Section 4 presents the results of our simulations and their corresponding discussions; finally, the key conclusions are drawn in Section 5.

2. The neural transverse-field Hopfield model

We view the neuronal system as a two-qubit network ruled by a neural transverse-field Hamiltonian.[28,43] This approach allows us to consider in one go how classical associative memory, quantum information processing and environmental interactions influence each other, sometimes favorably and sometimes unfavorably. A neuron is thought of as a qubit with its basis states corresponding to the firing and non-firing conditions, and we utilize the standard Pauli operators $\sigma_{j\alpha}$ to depict these degrees of freedom, with j being the neuron index in $\{1,2\}$ and α the operator type in $\{x,y,z\}$. The coherent dynamics are realized through the total Hamiltonian that incorporates the fundamental elements of computation and control,

$$H_{\text{total}} = H_{\text{mem}} + H_{\text{trans}} + H_{\text{bias}} + H_{xy}. \tag{1}$$

Each contribution isolates a distinct physical role, memory storage, quantum processing, local asymmetries and direct exchange interactions, which together set the stage for the behaviors we study.

We begin with the core memory component, H_{mem}, constructed as a tunable interpolation between a classical and a quantum associative memory pattern.[37,38] This design lets us change the character of the stored information in a controlled way and observe how that choice reshapes the subsequent dynamics,

$$\begin{aligned} H_{\text{mem}} &= (1-\alpha)H_{\text{class}} + \alpha H_{\text{quant}} \\ &= -(1-\alpha)J_{\text{hop}}\sigma_{1z}\sigma_{2z} - \alpha J_{\text{mem}}|\Phi^+\rangle\langle\Phi^+|. \end{aligned} \tag{2}$$

Here, H_{class} is the classical memory, an Ising-like interaction with coupling strength J_{hop} that energetically favors aligned neuron states, $|00\rangle$ or $|11\rangle$, in close analogy with the Hebbian rule in the classical Hopfield model.[25,26] In contrast, H_{quant} encodes a quantum memory pattern through a projector onto the maximally entangled Bell state $|\Phi^+\rangle = (|00\rangle + |11\rangle)/\sqrt{2}$ with energy scale J_{mem}. The dimensionless mixing parameter $\alpha \in [0,1]$ moves the memory continuously from purely classical, $\alpha = 0$, to purely quantum, $\alpha = 1$, and therefore provides a direct tuning knob to compare storage and recall across regimes.

We then introduce the quantum processing or tunneling term, H_{trans}. This term injects coherent dynamics by applying a uniform transverse magnetic field of strength Γ,

$$H_{\text{trans}} = -\Gamma(\sigma_{1x} + \sigma_{2x}). \tag{3}$$

The transverse field does not commute with the σ_z based memory terms, so it creates a genuine competition: on the one hand it tends to delocalize the system into superpositions and to mediate transitions between configurations, on the other hand the memory interaction tends to stabilize the stored patterns.[29,31] In effect, this is the engine that powers quantum annealing,[30,44] and it is central to any computational advantage one might hope to obtain from a quantum neural architecture.

Realistic implementations rarely enjoy perfect symmetry, so we include a bias term, H_{bias}, and a direct exchange term, H_{xy}, to reflect imperfections and crosstalk that are common in hardware. The bias introduces local magnetic fields on each neuron,

$$H_{\text{bias}} = -B_1\sigma_{1z} - B_2\sigma_{2z}, \tag{4}$$

with B_1 and B_2 setting the strengths of the local fields. These biases can break symmetry, shift effective thresholds and tilt the energy landscape in favor of particular firing states. The exchange interaction captures direct spin exchange between the qubits,

$$H_{xy} = \kappa_{xy}(\sigma_{1x}\sigma_{2x} + \sigma_{1y}\sigma_{2y}), \tag{5}$$

where κ_{xy} is the coupling strength. Such interactions are standard in many physical qubit platforms and they can strongly influence correlation buildup, synchronization and information flow across the pair.[45,46]

The system is initialized in a state that represents a well-defined quantum memory pattern. Practically, we imagine a write-in stage in which the system is brought into thermal equilibrium with a low-temperature reservoir under a strong memory encoding Hamiltonian $H_{\text{store}} = -J_{\text{store}}|\Phi^+\rangle\langle\Phi^+|$. The corresponding Gibbs state is

$$\rho(0) = \frac{1}{Z_{\text{store}}} \exp\left(-\frac{H_{\text{store}}}{k_B T_{\text{init}}}\right) \tag{6}$$

with $Z_{\text{store}} = \text{Tr}[\exp(-H_{\text{store}}/k_B T_{\text{init}})]$ the partition function. For a sufficiently low initial temperature T_{init}, the preparation yields a nearly pure Bell state, $\rho(0) \approx |\Phi^+\rangle\langle\Phi^+|$, which we take as the starting point for the dynamical study. This initialization isolates the role of subsequent processing and noise, since the stored pattern is cleanly defined at $t = 0$.

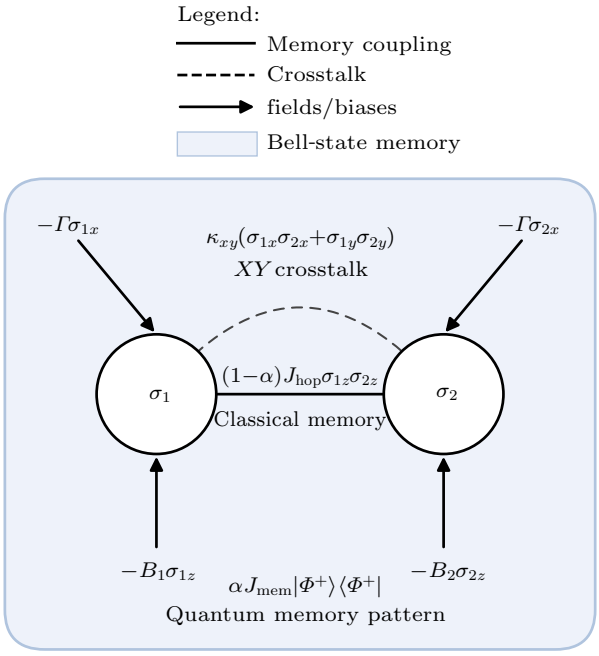


Fig. 1. Schematic representation of the two-neuron NTFH model. The neurons are represented by qubits σ_1 and σ_2. The solid horizontal link depicts the classical associative memory term $(1-\alpha)J_{\text{hop}}\sigma_{1z}\sigma_{2z}$, while the shaded blue background represents the quantum memory projector $\alpha J_{\text{mem}}|\Phi^+\rangle\langle\Phi^+|$, which favors a maximally entangled Bell state. The dashed curved line indicates XY-type crosstalk interaction κ_{xy}. External control is applied via transverse magnetic fields $-\Gamma\sigma_{jx}$ (diagonal arrows), which drive coherent tunneling, and longitudinal bias fields $-B_j\sigma_{jz}$ (vertical arrows), which break the local symmetry. The interplay between these coherent couplings and the environmental dissipation determines the stability of the stored quantum pattern.

2.1. Open system dynamics under environmental dephasing

To model a realistic neuronal environment, we must include the inevitable coupling between the two-qubit system and its surroundings. Such coupling leads to decoherence, the gradual loss of phase coherence and a drift toward more classical behavior. We treat the dynamics within the open system framework based on the Lindblad master equation, which is appropriate under the Born–Markov approximation.[32,47] In this setting, the environmental correlation time is short compared with the intrinsic evolutionary timescale, so memory effects in the bath can be neglected, a condition often met in complex biological and solid state environments.[48]

The time evolution of the density matrix $\rho(t)$ is then

$$\frac{\mathrm{d}\rho(t)}{\mathrm{d}t} = -\mathrm{i}[H_{\text{total}}, \rho(t)] + \sum_{j=1,2} \mathcal{D}[L_j]\rho(t). \tag{7}$$

The first term, $-\mathrm{i}[H_{\text{total}}, \rho(t)]$, describes coherent, unitary motion generated by the total Hamiltonian, with $\hbar = 1$. The second term encodes dissipative, non-unitary effects due to the environment. For each channel j, the dissipator has the standard Lindblad form[35,36]

$$\mathcal{D}[L_j]\rho(t) = \gamma_j \left(L_j \rho(t) L_j^\dagger - \frac{1}{2}\{L_j^\dagger L_j, \rho(t)\}\right). \tag{8}$$

The operators L_j specify how the bath acts on the system and the rates γ_j set the strength of those processes. In this work, we focus on pure dephasing, also called phase damping, which suppresses the off-diagonal elements of ρ in the energy eigenbasis without changing populations. For our two-qubit model, we take local dephasing channels on each neuron with $L_j = \sigma_{jz}$ and dephasing rates $\gamma_{\phi j}$. This master equation gives a complete and physically consistent baseline for simulating how quantum correlations evolve and decay when the model is exposed to realistic noise.

3. Quantification of correlations and uncertainty

To capture the full texture of the dynamics in our two-neuron quantum system, we track three complementary quantities. Together they let us follow the strongest quantum link through entanglement, the broader layer of non classical correlations through quantum discord, and the operational limits on predictability through an information theoretic notion of uncertainty. Using this trio side by side helps us separate how structure in the state supports computation from how noise and competition between terms in the Hamiltonian degrade that structure over time.

3.1. Entanglement of formation

Entanglement is a central resource in quantum mechanics and underpins many protocols in quantum information processing.[39] We quantify the entanglement shared by the two neuron qubits with EOF, which measures the minimum number of maximally entangled Bell pairs needed to assemble a target state using only local operations and classical communication.[49] For any two-qubit density matrix ρ, EOF is a monotonic function of the concurrence $C(\rho)$,[50] so once the concurrence is known, the entanglement scale follows directly.

The concurrence is computed as

$$C(\rho) = \max(0, \lambda_1 - \lambda_2 - \lambda_3 - \lambda_4), \tag{9}$$

where λ_i are the square roots of the eigenvalues of the matrix $R = \rho(\sigma_y \otimes \sigma_y)\rho^*(\sigma_y \otimes \sigma_y)$ in descending order. The corresponding EOF is set by the binary entropy evaluated at a function of the concurrence,

$$\mathrm{EOF}(\rho) = h\left(\frac{1+\sqrt{1-C^2(\rho)}}{2}\right), \tag{10}$$

where $h(x) = -x\log_2(x) - (1-x)\log_2(1-x)$. On this scale, $\mathrm{EOF} = 0$ indicates a separable state and $\mathrm{EOF} = 1$ indicates a maximally entangled state, such as a Bell state. This provides a clear and comparable readout of entanglement at each point in the evolution.

3.2. Geometric quantum discord

Entanglement does not exhaust the space of quantum correlations. Certain mixed states carry non-classical structure even when they are not entangled, and quantum discord is designed to reveal that broader layer.[51,52] We use GQD because it offers a geometric viewpoint: it is the minimum distance, measured by the Hilbert–Schmidt norm, between a given state and the set of classical quantum states that have zero discord.[40] This perspective pairs well with our open system setting, since geometry is often robust to small perturbations and provides intuition about how correlations are reshaped by noise.

For an arbitrary two-qubit state ρ, GQD admits an analytical expression

$$\mathrm{GQD}(\rho) = \frac{1}{4}\left(\|\vec{x}\|^2 + \|T\|_{\mathrm{HS}}^2 - \lambda_{\max}(K)\right), \tag{11}$$

where $\vec{x}_i = \mathrm{Tr}(\rho(\sigma_i \otimes I))$ is the Bloch vector of the first qubit, $T_{ij} = \mathrm{Tr}(\rho(\sigma_i \otimes \sigma_j))$ is the correlation tensor, $\|\cdot\|_{\mathrm{HS}}$ denotes the Hilbert–Schmidt norm and $\lambda_{\max}(K)$ is the largest eigenvalue of the 3×3 matrix $K = \vec{x}\vec{x}^{\mathrm{T}} + TT^{\mathrm{T}}$. In our context, GQD complements EOF by remaining informative in regimes where entanglement has already collapsed, thereby indicating residual quantum correlations that can still influence performance.[53]

3.3. Quantum memory-assisted entropic uncertainty

The uncertainty principle, originally framed in terms of standard deviations for non-commuting observables,[54] can be cast more sharply with entropy.[55,56] In this form, the theory sets a lower bound on our ability to predict the outcomes of two incompatible measurements. That bound changes when the measured system shares correlations with a quantum memory, since information stored in the memory can reduce uncertainty about measurement results.[57]

This idea is formalized by the quantum memory-assisted EUR relation due to Berta *et al.*[41] For a bipartite system AB, Alice measures one of two observables, for example σ_x or σ_z, on subsystem A, while Bob holds the memory B. The conditional entropies satisfy

$$S(X|B) + S(Z|B) \geq S(A|B) + c, \tag{12}$$

where $S(X|B) = S(\rho_{XB}) - S(\rho_B)$ is the conditional von Neumann entropy of the post measurement state ρ_{XB}, $S(A|B)$ is the conditional entropy of the initial state and c quantifies the incompatibility of the measurements. The inequality tells us how much the shared correlations can lower Alice's uncertainty in principle.

In our study, we use the left-hand-side of this relation as a direct diagnostic,

$$\mathrm{EUR}(\rho) = S(X|B) + S(Z|B). \tag{13}$$

Small values of EUR indicate that Bob's memory is highly informative about Alice's outcomes, which is a signature of strong correlations between A and B. Large values indicate weaker sharing of information and greater unpredictability. Read alongside EOF and GQD, EUR helps separate loss of coherence from loss of predictability, and it clarifies how the environment reshapes operational uncertainty in real time.

4. Results and discussion

In this section, we present and interpret the outcomes of our numerical simulations, with an emphasis on how the physical parameters of the NTFH model shape the time dependence of quantum correlations and uncertainty. We initialize the two-neuron system in a nearly pure, maximally entangled Bell state, $|\Phi^+\rangle$, so that the initial EOF and GQD are both close to 1.0, while the entropic uncertainty, EUR, is near 0. This starting point represents an ideal quantum memory pattern stored in the network, and it allows us to cleanly separate what is erased by the environment from what is scrambled by coherent processing. The subsequent evolution shows a nuanced competition between the coherent dynamics generated by the Hamiltonian and the dissipative action of environmental dephasing, revealing regimes where memory is slowly washed out and regimes where it is actively disrupted.

All simulations are performed in dimensionless units, taking the Hopfield coupling $J_{\rm hop}$ as the reference energy scale so that time is measured in units of $1/J_{\rm hop}$ and all other parameters appear as ratios to $J_{\rm hop}$ and $J_{\rm mem}$. The mixing parameter α sets the balance between the classical Ising term and the Bell-state projector in $H_{\rm mem} = (1-\alpha)H_{\rm class} + \alpha H_{\rm quant}$. The limits $\alpha = 0$ and $\alpha = 1$ correspond, respectively, to a purely classical Hopfield-type memory and to a purely quantum memory that selects a maximally entangled pattern.[37,38] We therefore choose representative values $\alpha = 0.1, 0.7, 0.9$ to sample classical-dominated, mixed and quantum-dominated regimes within a single framework. The transverse-field strength Γ is treated as the main control parameter driving coherent tunneling between stored configurations, in analogy with transverse-field Ising models used in quantum annealing.[28–30] To contrast weak and strong driving, we consider Γ much smaller than, comparable to and larger than $J_{\rm hop}$, e.g., $\Gamma = 0.1$, 0.8, 1.5, which respectively model perturbative, competitive and strongly disruptive transverse fields. The pure dephasing rate γ_ϕ fixes the timescale on which quantum coherences are suppressed by the environment in the Markovian Lindblad description.[32,48] We explore the range $\gamma_\phi/J_{\rm hop} \sim 10^{-2}$–$10^{-1}$ in order to span qualitatively distinct regimes: weak noise (e.g., $\gamma_\phi = 0.01$), where several coherent oscillations occur before decoherence dominates, and stronger noise (e.g., $\gamma_\phi = 0.10$), where the quantum-to-classical crossover takes place on a timescale comparable to a few intrinsic oscillation periods.

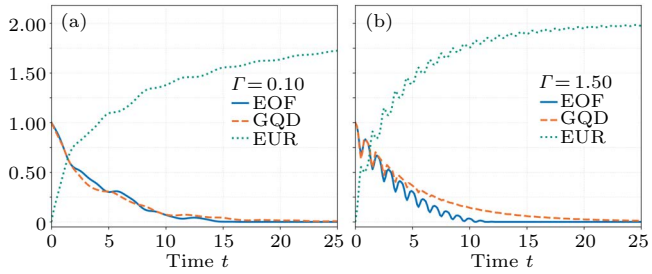


Fig. 2. Dynamics of entanglement of formation (EOF, solid blue), geometric quantum discord (GQD, dashed orange) and entropic uncertainty (EUR, dotted green) as functions of the transverse-field strength Γ. Panel (a) shows a weak field, $\Gamma = 0.1$, where the initial quantum memory state degrades slowly due to environmental noise. Panel (b) shows a strong field, $\Gamma = 1.5$, where rapid quantum tunneling destroys the initial memory but creates transient correlations through coherent oscillations. Other parameters are from the base set: $\alpha = 0.7, J_{\rm hop} = 1.0, J_{\rm mem} = 1.2, B_2 = 0.1, \kappa_{xy} = 0.2, \gamma_\phi = 0.03$.

Figure 2 highlights the governing role of the transverse-field strength Γ, which sets the pace of quantum tunneling. In the weak-field regime (Fig. 2(a), $\Gamma = 0.1$), coherent motion is slow and environmental dephasing dominates. Starting near their maxima, EOF and GQD decay smoothly and monotonically toward zero over a timescale of approximately $t = 10$. In parallel, EUR rises gradually from its initial value near zero to a high steady state near 1.75, which signals a steady loss of predictive power as the quantum memory fades under decoherence. In sharp contrast, the strong-field regime (Fig. 2(b), $\Gamma = 1.5$) exhibits fast, high-frequency oscillations in all three diagnostics. Here the transverse field competes directly with the memory term and actively scrambles the initially stored pattern, so the running averages of EOF and GQD drop much more quickly, even though periodic revivals briefly restore correlations through coherent motion. EUR increases rapidly and oscillates out of phase with the correlation measures, approaching a final level with even higher uncertainty, EUR ≈ 2.0. The comparison shows that a weak field lets the environment slowly erase memory whereas a strong field accelerates loss by driving the system away from the stored state through its own coherent dynamics.

Figure 3 examines how the intrinsic character of memory, set by α, reshapes the dynamics. For a predominantly quantum memory (Fig. 3(b), $\alpha = 0.9$), the initial state $|\Phi^+\rangle$ aligns with the memory Hamiltonian, so correlations start near their maxima (EOF and GQD ≈ 1.0, with EUR ≈ 0). This state is delicate, the combination of transverse driving and noise produces large-amplitude oscillations and a rapid decay of both entanglement and discord, which almost vanish by $t = 15$. EUR rises quickly in tandem, reflecting the swift loss of predictive power. For a predominantly classical memory (Fig. 3(a), $\alpha = 0.1$), the same initial entangled state is a high-energy, unstable configuration relative to the classically dominated Hamiltonian. The system still begins with notable correlations inherited from preparation, yet these correlations are less pronounced and decay from a lower effective peak. The oscillations are smaller, and the long-time decay of GQD is more gradual. The system drifts toward a configuration that is more resilient to dephasing, which acts in the same basis as the classical Ising interaction. The comparison exposes a basic tradeoff, a quantum native memory stores stronger correlations at $t = 0$ but is highly sensitive to perturbations, while a classically oriented memory is less entangled yet more durable under the same noise.

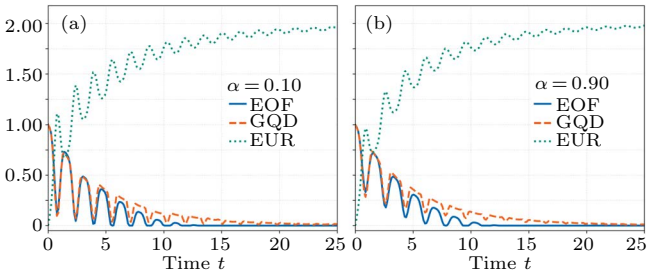


Fig. 3. Dynamics for different memory mixing parameters α. Panel (a) shows a predominantly classical memory ($\alpha = 0.1$), which has low initial entanglement but is robust against decoherence. Panel (b) shows a predominantly quantum memory ($\alpha = 0.9$), which starts in a highly entangled state that is fragile and decays quickly under the influence of the transverse field and noise. Other parameters: $\Gamma = 0.8, J_{\rm hop} = 1.0, J_{\rm mem} = 1.2, B_2 = 0.1, \kappa_{xy} = 0.2, \gamma_\phi = 0.03$.

Figure 4 isolates the effect of an XY-type interaction, or crosstalk, set by κ_{xy}. The baseline case in Fig. 4(a) ($\kappa_{xy} = 0.0$) shows the familiar pattern, EOF and GQD begin near 1.0, then oscillate and decay as the transverse field drives coherent motion and the environment damps it, both measures approaching zero by $t \approx 15$, while EUR climbs toward a steady level near 2.0. With strong crosstalk (Fig. 4(b), $\kappa_{xy} = 1.0$), the long-term fate is unchanged and correlations still vanish. The transient structure, however, is clearly different: all three curves oscillate with higher and more complex frequencies. The added two-qubit interaction reshapes the energy spectrum and therefore the gaps that set the oscillation periods. Crosstalk does not halt decoherence, it redirects the coherent pathway taken as the system loses its quantum features, which illustrates how additional internal couplings can tune the choreography of information flow without ultimately saving the stored pattern.

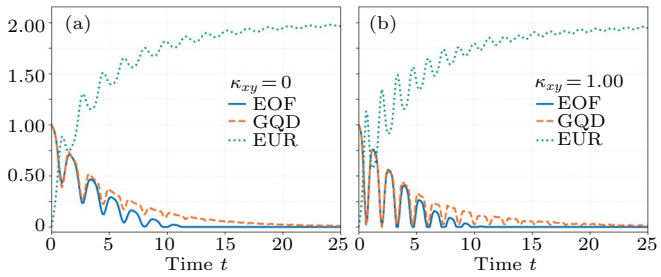


Fig. 4. Dynamics for different XY crosstalk strengths κ_{xy}. Panel (a) shows no crosstalk ($\kappa_{xy} = 0.0$), displaying the baseline dynamics. Panel (b) shows strong crosstalk ($\kappa_{xy} = 1.0$), which introduces an additional coherent interaction that competes with the memory Hamiltonian and modifies the oscillation frequencies and the stability of quantum correlations. Other parameters: $\Gamma = 0.8, \alpha = 0.7, J_{\text{hop}} = 1.0, J_{\text{mem}} = 1.2, B_2 = 0.1, \gamma_\phi = 0.03$.

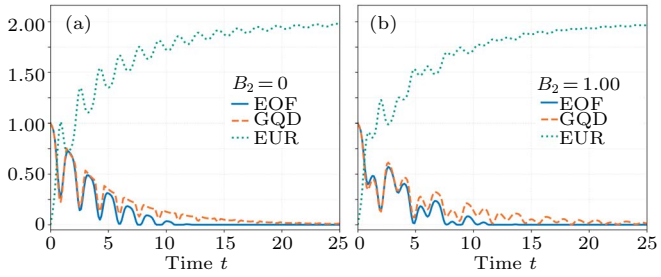


Fig. 5. Dynamics for different asymmetric bias fields on the second neuron. Panel (a) shows a symmetric system ($B_2 = 0.0$) allowing for sustained coherent dynamics. Panel (b) shows a strong local bias ($B_2 = 1.0$), which breaks the symmetry and effectively localizes the second qubit state. This projection rapidly destroys all shared correlations, both EOF and GQD, causing a sharp increase in uncertainty. Other parameters: $\Gamma = 0.8, \alpha = 0.7, J_{\text{hop}} = 1.0, J_{\text{mem}} = 1.2, \kappa_{xy} = 0.2, \gamma_\phi = 0.03$.

Figure 5 makes the destructive impact of local asymmetry explicit. With perfect symmetry (Fig. 5(a), $B_2 = 0.0$), the system supports robust oscillations and correlations decay gradually under environmental action. With a strong bias applied only to the second neuron (Fig. 5(b), $B_2 = 1.0$), the effect is sudden and severe. EOF and GQD collapse from near 1.0 to almost zero within a short interval of approximately $t = 2$, and coherent oscillations are nearly extinguished. EUR jumps almost instantly from 0 to above 1.5, which signals a swift loss of predictive power. Physically, the term $-B_2\sigma_{2z}$ breaks exchange symmetry and energetically pins the second neuron in a definite σ_{2z} eigenstate. This localization resembles a continuous projective measurement on the second qubit, and because entanglement and discord require a shared, indefinite state, fixing one part of the pair destroys nonlocal correlations for the whole. The result underscores how sensitive quantum resources are to local, non-uniform perturbations, and it points to a practical constraint for devices where constituent elements cannot be perfectly matched.

Next, we intend to examine the role of dephasing in our specific chosen model. To verify that our conclusions are not tied to a specific noise strength, we explicitly simulate the dynamics for several dephasing rates γ_ϕ (Fig. 6). In particular, we compare a weakly coupled regime ($\gamma_\phi = 0.01$), where entanglement and discord exhibit long-lived oscillations, with a strongly dephasing regime ($\gamma_\phi = 0.10$), where all quantum correlations are rapidly destroyed and the entropic uncertainty saturates to its maximal value. Intermediate values (such as $\gamma_\phi = 0.03$ used in our base parameter set) interpolate smoothly between these limits, confirming that the qualitative behavior we report is robust under variations of the environmental dephasing rate.

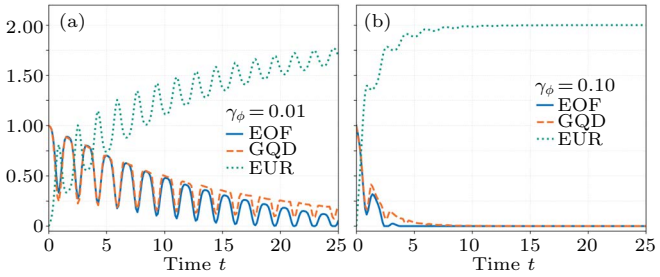


Fig. 6. Dynamics for different environmental dephasing rates γ_ϕ. Panel (a) shows weak environmental coupling ($\gamma_\phi = 0.01$), where quantum correlations persist for a long time. Panel (b) shows strong coupling ($\gamma_\phi = 0.10$), where environmental noise rapidly destroys both entanglement and discord, leading to a purely classical mixed state and high uncertainty. Other parameters: $\Gamma = 0.8, \alpha = 0.7, J_{\text{hop}} = 1.0, J_{\text{mem}} = 1.2, B_2 = 0.1, \kappa_{xy} = 0.2$.

Finally, figure 6 provides a direct view of environmental decoherence controlled by the dephasing rate γ_ϕ. Under weak coupling (Fig. 6(a), $\gamma_\phi = 0.01$), the environment perturbs gently and intrinsic coherent dynamics dominate for an extended interval. EOF and GQD display large, sustained oscillations whose amplitudes decay slowly, and both remain non-zero through the full simulation, still present at $t = 25$. EUR oscillates with a slowly rising baseline, never reaching its theoretical maximum. This is a high-coherence setting where quantum processing is viable over long times. Under strong coupling (Fig. 6(b), $\gamma_\phi = 0.10$), decoherence overwhelms coherent motion. Oscillations are suppressed, EOF and GQD plummet from near maximal values to remain at zero by $t \approx 5$, and EUR rises swiftly and monotonically to its maximum value of 2.0, where it stays. The contrast is a clear demonstration of the

quantum to classical transition driven by noise and it stresses the importance of environmental isolation for preserving the quantum resources that computation relies upon.

Taken together, these results reveal a consistent picture. The transverse field is a double-edged control, it powers coherent exploration that can aid processing yet it also scrambles stored patterns when it is too strong. The nature of memory, set by α, balances quality against resilience, quantum-dominant storage begins stronger and fails faster, classical-dominant storage begins weaker and lasts longer. Additional coherent couplings such as κ_{xy} retune the spectrum and the transient choreography without changing the end state dictated by noise. Local asymmetries, exemplified by B_2, are especially harmful, since they act as effective measurements that collapse shared structure. Environmental dephasing, set by γ_ϕ, finally determines whether the system explores meaningfully before damping or falls immediately into classical mixtures. For design, the message is practical, moderate transverse drive, careful symmetry control and low dephasing rates are essential if a neural-inspired quantum memory is to retain useful correlations on operational timescales.

4.1. Quantum phase transition in a multi-neuron system

To probe collective behavior and the possibility of emergent phenomena in a larger network, we extend our analysis to a four-qubit system ($N = 4$). This step lets us examine a quantum phase transition (QPT), a central idea in many-body physics in which the ground state of a system changes its qualitative character at zero temperature when a control parameter is tuned.[42] In our setting, the transverse-field strength Γ plays the role of that tuning knob, and it allows us to move continuously between an ordered, memory-dominated regime and a regime where quantum tunneling prevails.

The Hamiltonian for the N-qubit model is a streamlined generalization of the two-qubit case that preserves the primary competition between memory and transverse drive,

$$\begin{aligned} H_N &= (1-\alpha)H_{\text{class}} + \alpha H_{\text{quant}} + H_{\text{trans}} \\ &= -(1-\alpha)J_{\text{hop}}\sum_{i<j}^{N}\sigma_{iz}\sigma_{jz} - \alpha J_{\text{mem}}|\text{GHZ}\rangle\langle\text{GHZ}| - \Gamma\sum_{i=1}^{N}\sigma_{ix}, \end{aligned} \tag{14}$$

where the classical term implements an all-to-all ferromagnetic interaction and the quantum term projects onto the N-qubit GHZ state $|\text{GHZ}\rangle = (|00\cdots0\rangle + |11\cdots1\rangle)/\sqrt{2}$. To isolate the universal features of the QPT, we omit local bias and XY crosstalk terms in this section, so the transition can be attributed cleanly to the balance between storage and tunneling.

The QPT is encoded in the ground state structure of H_N. Rather than following time evolution, we solve the time-independent Schrödinger equation $H_N|\psi_n\rangle = E_n|\psi_n\rangle$ by exact diagonalization of Eq. (14). Our analysis centers on the ground state $|\psi_0\rangle$ and the first excited state $|\psi_1\rangle$, with energies E_0 and E_1, because their separation and response to Γ capture the onset of criticality in a finite system and reveal how memory competes with delocalization.

Figure 7 summarizes the ground state analysis and provides converging evidence for a second-order QPT. Figure 7(a) presents two classic indicators. First, the gap $\Delta E = E_1 - E_0$ that protects the ground state narrows and reaches a non-zero minimum at the finite size critical point Γ_c. Second, the magnetic susceptibility

$$\chi_x = -\frac{\partial\langle M_x\rangle}{\partial\Gamma} = -\frac{\partial}{\partial\Gamma}\left(\frac{1}{N}\langle\psi_0|\sum_{i=1}^{N}\sigma_{ix}|\psi_0\rangle\right) \tag{15}$$

shows a sharp negative minimum at the same field, which marks a maximal rate of change in the alignment with the transverse drive and locates the phase boundary with high precision.

Figure 7(b) turns to quantum correlations. Here we compute the bipartite EOF by tracing out two of the four qubits from the ground state $\rho_0 = |\psi_0\rangle\langle\psi_0|$ and then applying the definition from Section 3. Across values of α a common pattern emerges: entanglement grows and peaks at or very near Γ_c. This behavior ties the strengthening of quantum correlations directly to the region where ordering and disordering tendencies compete most intensely. Notably, the location of the peak drifts toward larger Γ as the memory becomes more quantum, that is, as α increases from 0.1 to 0.9, which reflects the increased field strength required to disrupt an ordered phase rooted in a more quantum memory projector.

Figure 7(c) gathers these observations into a phase diagram in the α–Γ plane. The boundary $\Gamma_c(\alpha)$ separates an ordered memory phase at low Γ from a paramagnetic phase at high Γ, and the dependence on α is non-monotonic. The critical field increases with α at first, reaches a maximum near intermediate mixing around $\alpha \approx 0.7$, then decreases. This means that the hybrid memory structure, neither purely classical nor purely quantum, can provide the greatest robustness against the disordering action of the transverse field in this finite system.

Figure 7(d) assesses the order of the transition through the ground state energy density E_0/N. The curve itself is smooth across Γ_c, while its second derivative $-\partial^2(E_0/N)/\partial\Gamma^2$ displays a sharp positive peak. By the Hellmann–Feynman theorem, this curvature is directly tied to the response encoded by Eq. (15), and indeed the peak matches the negative minimum of χ_x in Fig. 7(a). Taken together, these signatures confirm a second-order QPT in the multi-neuron Hopfield model and establish a clear link between neural memory concepts and the standard framework of quantum criticality in many-body systems.

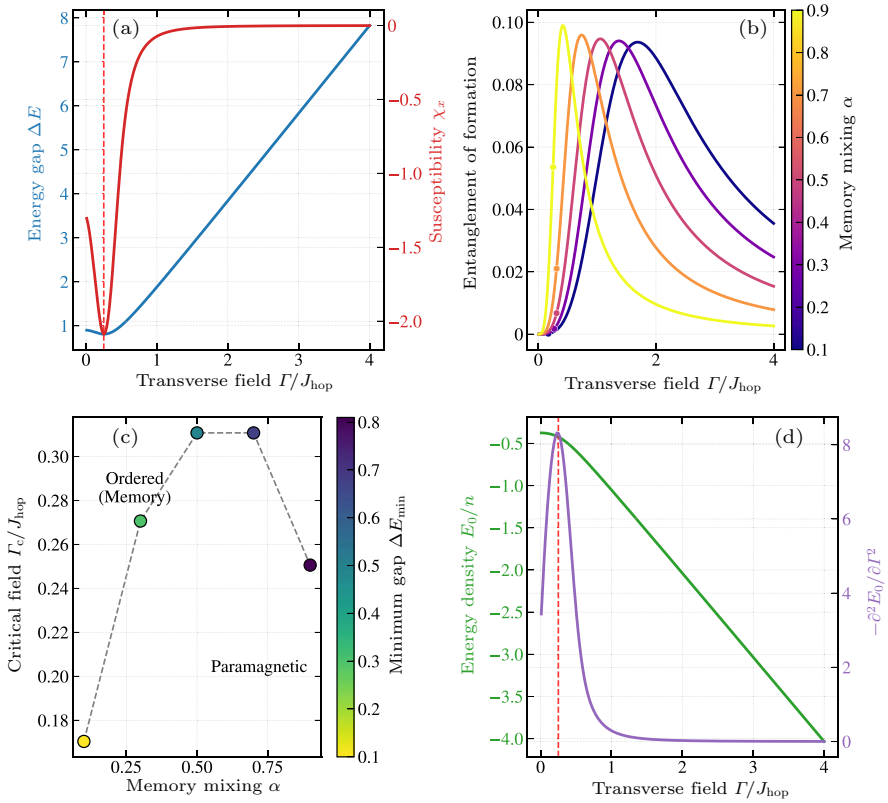


Fig. 7. Quantum phase transition analysis for the four-qubit neural Hopfield model. The panels display standard signatures of a QPT driven by the transverse field Γ. (a) For a representative case the energy gap ΔE in blue approaches a minimum at a critical point Γ_c, at the same location the magnetic susceptibility χ_x in red shows a sharp negative extremum. (b) The bipartite EOF between two neurons is shown for several memory mixing parameters α, the entanglement peaks in the neighborhood of the critical point for each α. (c) The quantum phase diagram plots the non-monotonic critical field Γ_c as a function of α, the color bar records the size of the minimum gap, and the boundary separates an ordered, memory-dominated phase at low Γ from a disordered, paramagnetic phase at high Γ. (d) The ground state energy density E_0/N in green is continuous, while its second derivative $-\partial^2 E_0/\partial\Gamma^2$ in purple is singular at Γ_c, which is consistent with a second-order transition.

Although our explicit simulations focus on a two-qubit open system and a four-qubit closed network, the underlying mechanisms are expected to extend to larger architectures. In particular, the competition between memory interactions, transverse fields and dephasing that controls the trade-off between storage and processing should persist in generic N-qubit networks, while the transverse-field-driven quantum phase transition observed for $N = 4$ is the finite-size precursor of a standard thermodynamic transition in the large-N limit.[42] Scaling up mainly affects quantitative aspects, such as critical fields, gaps and correlation lengths, which may be accessed with tensor-network, mean-field or Monte Carlo techniques, but the qualitative picture of a fragile quantum neural memory subject to competing coherent and dissipative processes remains unchanged.

Beyond the minimal architectures considered here, our study suggests several natural directions for future work. On the theoretical side, it would be important to explore larger networks and more realistic connectivity patterns (e.g., sparse, modular, or hierarchical graphs) to assess how quantum neural memory scales with system size and topology. Incorporating non-Markovian environments and structured noise could clarify whether memory effects in the bath can stabilize or, conversely, further destabilize quantum correlations in neuro-inspired hardware. From a more applied perspective, embedding the NTFH model into concrete quantum platforms (such as superconducting qubits, trapped ions or Rydberg arrays) and benchmarking its performance against classical Hopfield networks would help determine to what extent quantum-enhanced associative memory can be realized in practice.

5. Conclusion

We have conducted a comprehensive theoretical investigation of a neural transverse-field Hopfield model, and analyzed its dynamic behavior in a minimal open system as well as its static properties in a small many-body setting. By depicting a two-neuron circuit as an open quantum system, we have measured the evolution of quantum correlations and uncertainty under coherent driving, environmental noise and controlled imperfections. The main points arising from this investigation highlight the subtlety of quantum resources in such systems. The transverse field has a double function, it assists the computation by allowing quantum tunneling and at the same time it causes a particular storing pattern to become unstable. The specific nature of memory creates a clear trade-off, a quantum-dominant pattern has a higher-fidelity entanglement at the start but is more fragile, while the classical-

oriented pattern has lower initial quantum character but can survive noise for a longer period. Moreover, we have detected a strong local asymmetric bias as a very vulnerable point, which can lead to almost immediate collapse of correlations, in addition to the slower yet inevitable degradation caused by environmental dephasing.

Although our model is deliberately basic compared with biological reality, it still acts as a rigorous theoretical laboratory. This model serves as a point of reference for the assessment of how internal interactions, external fields and environmental channels are responsible for the emergence, sustainability and extinction of quantum resources in the designs that are inspired by neurotechnology. The natural gradients are to cause larger N, to get to the thermodynamic limit and to assess all the possible topologies beyond all-to-all coupling and to take into consideration non-Markovian structures in the environment that may be a better representation of biological media. In brief, this research makes the organizing principles at the boundaries of statistical mechanics, quantum information and neural computation explicit, and it provides specific paths through which quantum-enhanced methods in memory and processing can be created and their effectiveness verified.

Acknowledgements

This work was supported by the Fundamental Research Funds for the Central Universities, the National Natural Science Foundation of China (Grant No. 31571042), Beijing Municipal Natural Science Foundation (Grant No. 7202129), the Class B Breeding Program of Special Projects for Leading Science and Technology of the Chinese Academy of Sciences (Grant No. XDPB16), and the Key Basic Research Project of Applied Basic Research Program of Hebei Province (Grant No. 18966315D).

References

[1] Churchland P S and Sejnowski T J 1992 *The Computational Brain* (Cambridge, MA: MIT Press)
[2] Koch C 1999 *Biophysics of Computation: Information Processing in Single Neurons* (New York: Oxford University Press)
[3] Dayan P and Abbott L F 2001 *Theoretical Neuroscience: Computational and Mathematical Modeling of Neural Systems* (Cambridge, MA: MIT Press)
[4] Ermentrout B and Terman D M 2010 *Mathematical Foundations of neuroscience* (Vol. 35). New York: springer)
[5] Ullah I, Khan S, Noman M and Lang M 2026 *International Journal of Modern Physics A* **41** 2650035
[6] LeCun Y, Bengio Y and Hinton G 2015 *Nature* **521** 436
[7] Von Neumann J and Kurzweil R 2012 *The Computer and the Brain* (Yale University Press)
[8] Penrose R 1989 *The Emperor's New Mind: Concerning Computers, Minds, and the Laws of Physics* (Oxford: Oxford University Press)
[9] Aerts D 2009 *J. Math. Psychol.* **53** 314
[10] Busemeyer J R and Bruza P D 2012 *Quantum Models of Cognition and Decision* (Cambridge: Cambridge University Press)
[11] Pothos E M and Busemeyer J R 2013 *Behavioral and Brain Sciences* **36** 255
[12] Wang Z, Busemeyer J R, Atmanspacher H and Pothos E M 2013 *Top. Cogn. Sci.* **5** 672
[13] Haven E and Khrennikov A 2013 *Quantum Social Science* (Cambridge: Cambridge University Press)
[14] Khrennikov A 2010 *Ubiquitous Quantum Structure: From Psychology to Finance* (Berlin: Springer)
[15] Asano M, Basieva I, Khrennikov A, Ohya M, Tanaka Y and Yamato I 2011 *Phys. Rev. A* **84** 032120
[16] Tegmark M 2000 *Phys. Rev. E* **61** 4194
[17] Zurek W H 2003 *Rev. Mod. Phys.* **75** 715
[18] Rahman A U, Liu A X, Haddadi S and Qiao C F 2025 *Phys. Rev. D* **111** 064077
[19] Rahman A U and Qiao C F 2024 *Quantum Inf. Process.* **23** 315
[20] Penrose R 1996 *Shadows of the Mind: A Search for the Missing Science of Consciousness* (Oxford: Oxford University Press)
[21] Hameroff S and Penrose R 2014 *Phys. Life Rev.* **11** 39
[22] Fisher M P A 2015 *Ann. Phys.* **362** 593
[23] Kak S C 1995 *Inf. Sci.* **83** 143
[24] Schuld M, Sinayskiy I and Petruccione F 2014 *Quantum Inf. Process.* **13** 2567
[25] Hopfield J J 1982 *Proc. Natl. Acad. Sci. USA* **79** 2554
[26] Amit D J, Gutfreund H and Sompolinsky H 1985 *Phys. Rev. Lett.* **55** 1530
[27] Hertz J, Krogh A and Palmer R G 1991 *Introduction to the Theory of Neural Computation* (Reading, MA: Addison-Wesley)
[28] Nishimori H 2001 *Statistical Physics of Spin Glasses and Information Processing: An Introduction* (Oxford: Oxford University Press)
[29] Santoro G E, Martoňák R, Tosatti E and Car R 2002 *Science* **295** 2427
[30] Kadowaki T and Nishimori H 1998 *Phys. Rev. E* **58** 5355
[31] Das A and Chakrabarti B K 2008 *Rev. Mod. Phys.* **80** 1061
[32] Breuer H P and Petruccione F 2002 *The Theory of Open Quantum Systems* (Oxford: Oxford University Press)
[33] Mohamed A B A, Rahman A U and Eleuch H 2022 *Entropy* **24** 545
[34] Rahman A U, Liu A X, Abd-Rabbou M Y and Qiao C F 2025 arXiv:2511.10470
[35] Gorini V, Kossakowski A and Sudarshan E C G 1976 *J. Math. Phys.* **17** 821
[36] Lindblad G 1976 *Commun. Math. Phys.* **48** 119
[37] Fiebig H R and Fiebig H 2003 *Phys. Rev. E* **68** 016202
[38] Fujii K and Nakajima K 2017 *Phys. Rev. Appl.* **8** 024030
[39] Horodecki R, Horodecki P, Horodecki M and Horodecki K 2009 *Rev. Mod. Phys.* **81** 865
[40] Dakić B, Vedral V and Brukner Č 2010 *Phys. Rev. Lett.* **105** 190502
[41] Berta M, Christandl M, Colbeck R, Renes J M and Renner R 2010 *Nat. Phys.* **6** 659
[42] Sachdev S 2011 *Quantum Phase Transitions*, 2nd edn (Cambridge: Cambridge University Press)
[43] Rotondo G, Cosentino M, Gibilisco S and San Biagio P L 2018 *J. Phys. A: Math. Theor.* **51** 085302
[44] Farhi E, Goldstone J, Gutmann S and Sipser M 2001 *Science* **292** 472
[45] Kane B E 1998 *Nature* **393** 133
[46] Loss D and DiVincenzo D P 1998 *Phys. Rev. A* **57** 120
[47] Carmichael H J 1999 *Statistical Methods in Quantum Optics 1: Master Equations and Fokker–Planck Equations* (Berlin: Springer) **53** 78
[48] Schlosshauer M A 2007 *Decoherence and the Quantum-to-Classical Transition* (Berlin: Springer)
[49] Bennett C H, DiVincenzo D P, Smolin J A and Wootters W K 1996 *Phys. Rev. A* **54** 3824
[50] Wootters W K 1998 *Phys. Rev. Lett.* **80** 2245
[51] Ollivier H and Zurek W H 2001 *Phys. Rev. Lett.* **88** 017901
[52] Henderson L and Vedral V 2001 *J. Phys. A: Math. Gen.* **34** 6899
[53] Modi K, Brodutch A, Cable H, Paterek T and Vedral V 2012 *Rev. Mod. Phys.* **84** 1655
[54] Heisenberg W 1927 *Z. Phys.* **43** 172
[55] Deutsch D 1983 *Phys. Rev. Lett.* **50** 631
[56] Maassen H and Uffink J B M 1988 *Phys. Rev. Lett.* **60** 1103
[57] Renes J M and Boileau J C 2009 *Phys. Rev. Lett.* **103** 020402